

CrystEngComm

Accepted Manuscript



This is an *Accepted Manuscript*, which has been through the Royal Society of Chemistry peer review process and has been accepted for publication.

Accepted Manuscripts are published online shortly after acceptance, before technical editing, formatting and proof reading. Using this free service, authors can make their results available to the community, in citable form, before we publish the edited article. We will replace this *Accepted Manuscript* with the edited and formatted *Advance Article* as soon as it is available.

You can find more information about *Accepted Manuscripts* in the [Information for Authors](#).

Please note that technical editing may introduce minor changes to the text and/or graphics, which may alter content. The journal's standard [Terms & Conditions](#) and the [Ethical guidelines](#) still apply. In no event shall the Royal Society of Chemistry be held responsible for any errors or omissions in this *Accepted Manuscript* or any consequences arising from the use of any information it contains.

Lipid or Aqueous Medium for Hematin Crystallization?

Peter G. Vekilov^{a,b,*}, Jeffrey D. Rimer^{a,*}, Katy N. Olafson^a, Megan A. Ketchum^a

^a Department of Chemical and Biomolecular Engineering, University of Houston, 4800 Calhoun Road, Houston, Texas 77204, USA.

^b Department of Chemistry, University of Houston, 4800 Calhoun Road, Houston, Texas 77204, USA.

Corresponding authors:

Peter G. Vekilov

Department of Chemical and Biomolecular Engineering

University of Houston, 4800 Calhoun Blvd., Houston, TX 77204-4004, USA

Jeffrey D. Rimer

Department of Chemical and Biomolecular Engineering

University of Houston, 4800 Calhoun Blvd., Houston, TX 77204-4004, USA

Keywords: hematin crystallization; malaria parasites; heme detoxification; crystallization mechanisms; antimalarial drug solubility.

Abstract

Hematin crystallization is the primary heme detoxification mechanism of malaria parasites infecting human erythrocytes and the target of currently applied antimalarial medications. The composition of the crystallization medium within the parasite's digestive vacuole (DV), the aqueous or lipid sub-phases, has been the subject of intense debate. Here we show that a blend of lipids, designed to mimic the lipid sub-phase in the parasite DV, contains significant amounts of soluble water that facilitates hematin crystal formation. We show that the hematin solubility in citric buffer-saturated n-octanol (CBSO), a model for the DV lipid sub-phase, is 100,000-fold greater than in a biomimetic aqueous solution, indicating that organic-based crystallization provides an environment for faster hematin crystallization and more efficient heme detoxification. We demonstrate that hematin crystals grow with physiologically-relevant rates from CBSO and do not grow from our biomimetic aqueous solvents. Our findings suggest that hematin crystallization most likely requires the participation of lipid structures. We propose a mechanism of hematin crystallization in the parasite DV that reconciles this conclusion with data on hemoglobin transport and hematin generation and crystallization *in vivo*. The proposed mechanism suggests that hematin becomes incorporated into crystals via a layer of neutral lipids or possibly after penetrating the phospholipid bilayer of the DV. We specify guidelines for tests of the proposed mechanism and highlight its clinical and pharmacological implications.

Introduction

The main mechanism of heme detoxification in malaria parasites (i.e., *Plasmodium falciparum*, *Plasmodium vivax*, and three others) is the formation of hemozoin crystals. Parasites catabolize hemoglobin and release Fe(II) heme,¹ which oxidizes to toxic Fe(III) hematin. The cytotoxicity of hematin stems from two processes: hematin catalyzes the production of reactive oxygen species, and it binds to cell membranes. These processes can lead to severe cell structure

damage.² To survive, the parasites sequester hemozoin as crystalline hemozoin.^{3, 4} Accordingly, the traditional Western treatment for malaria, quinine, and its synthetic homologues (chloroquine, amodiaquine, and others)⁵⁻⁸, operate by inhibiting hemozoin crystallization.^{9,10}

Malaria is endemic in most equatorial regions of the world.¹¹ Approximately 584,000 million deaths, a subset of 124 to 283 million clinical episodes, are caused by malaria every year. Nearly 40% of the global population is at risk for malaria infection.¹² A resurgence of the disease has occurred in since 1970 and 80's due to the spread of *Plasmodium* parasites resistant to chloroquine combination treatments.^{11, 13} In recent years, parasite resistance to artemisinins, the most advanced line of antimalarial defense, has been detected in 5 countries of the Southeast Asia.¹² The weak responses to the common antimalarial drugs underscore the urgent need for research into the main processes of the malaria parasite physiology.

Despite many years of effort,^{4, 6, 9, 14-17} fundamental questions regarding the mechanism of hemozoin crystallization and its inhibition remain elusive. One of the most significant open questions is on the nature of the environment within the parasite where hemozoin crystals recruit hemozoin and grow. Hemoglobin digestion and heme detoxification occurs in the parasite digestive vacuole (DV), the organelle that ensures fast growth and replication of the parasite. While the majority of the DV volume is occupied by an aqueous solution with pH in the range 4.8 – 5.5,^{18, 19} lipids, mostly neutral mono- and diglycerides, have been reported to form a sub-phase in the DV bulk.^{6, 15, 20}

The origin of the lipids in the DV can be traced to the invasion of the erythrocyte by a merozoite, the parasite form that escapes the liver (the parasites settle in their host's liver following introduction by a mosquito).²¹ The merozoite enforces a localized indentation in the erythrocyte membrane, which deepens until the neck connecting the merozoite space with blood plasma is severed. Thus, the endocytosed parasite is completely surrounded by the erythrocyte membrane in addition to its own. The resulting double phospholipid bilayer defines the formation of the parasite DV and the transport of hemoglobin to the DV. The proposed scenarios of DV

formation and supply of hemoglobin^{22, 23} assume invagination of the parasite's double membrane to endocytose hemoglobin-rich erythrocyte cytoplasm.^{21, 22} The formed double-walled vesicles hold the remnants of the erythrocyte membrane on the inside. As several such vesicles fuse to form the DV, invading proteases and lipases digest hemoglobin to aminoacids and heme and convert the inner membrane phospholipids to neutral glycerides.²⁰

These scenarios suggest an estimate of the total amount of neutral lipids that may accumulate in the DV of a mature parasite. A parasite processes up to 70% of the total hemoglobin in a red blood cell.²⁴ The corresponding volume of the erythrocyte cytoplasm endocytosed and transported to the DV is ca. $V = 70$ fL (1 femtoLiter = 10^{-15} L = $1 \mu\text{m}^3$). Assuming that the hemoglobin transport vesicles are spheres of radius $r = 300$ nm,²⁵ and that each phospholipid molecule occupies $\delta S = 0.7$ nm² ²⁶ on a bilayer surface and yields one glyceride lipid molecule, we obtain $n = 6V/r\delta S \approx 2 \times 10^9$ as a rough estimate of the number of neutral lipid molecules. This value would be moderately altered by assuming larger or smaller transport vesicles. A sub-phase of this amount of glycerides would occupy a volume of ~ 1 fL, a relatively small fraction of the DV volume in a mature trophozoite (the parasite form that feeds on hemoglobin) of ca. 50 fL.^{22, 23} The volume of the lipid sub-phase may be further reduced by lipids that embed in the DV phospholipid bilayer.²⁷

The location and structure of the lipid sub-phase in the parasite DV is a subject of debate. Electron microscopy observations have indicated that the lipids, which poorly dissolve in water, self-assemble into nanospheres suspended in the DV.^{6, 15} However, recent studies with mature parasites suggest the absence of suspended lipid structures greater than 25 nm.^{17, 25, 28} It is feasible that a significant fraction of the neutral lipids deposit on the DV walls and thicken the DV membrane, as documented by Kapishnikov *et al.* ^{17, 25, 28} Hemozoin crystals have been observed immersed in the lipid nanospheres,^{6, 15} or with their basal surfaces attached to the DV membrane^{17, 25, 28} and other crystal faces apparently exposed to the acidic aqueous phase. While it is accepted that hemozoin crystals nucleate on the DV membrane,^{16, 25} disagreement as to the crystal growth

medium (aqueous or organic) and the pathways in which free hemozoin incorporates into the growing crystal is still rampant.^{17, 25, 28-31}

Here, we review recent evidence that suggests that hemozoin crystallization requires the participation of lipid structures. We demonstrate that a significant amount of water can be dissolved in a mixture of mono- and diglycerides that are representative of the physiological neutral lipid composition in the parasite DV. Based on the solubility of water in the lipid blend, we design a model solvent—citric buffer-saturated n-octanol (CBSO)—to mimic the lipid environment for hemozoin crystallization. We demonstrate that hemozoin solubility is ca. 10^5 higher in CBSO than in biomimetic aqueous solvents; that several common antimalarial drugs are soluble in CBSO at concentrations sufficient for their efficacy as crystal growth inhibitors; and that hemozoin crystals with structure and morphology identical to physiological hemozoin grow at physiologically-relevant rates from hemozoin solutions in CBSO, but not in biomimetic aqueous solvents. These findings demonstrate that hemozoin crystallization from a lipid phase is a significantly more efficient route for heme detoxification and suggest that the lipid sub-phases in the parasite DV's may be the location for hemozoin crystallization. We propose a scenario that reconciles this conclusion with the available observations of hemoglobin digestion, hemozoin generation, and heme detoxification *in vivo*.

The water content of the lipid sub-phase in the parasite DV

Both physiological and synthetic hemozoin crystals are comprised of dimers bound by reciprocal COO⁻-Fe(III) coordination bonds, and connected through chains of -COOH-HOOC- hydrogen bonds.⁴ The formation of hydrogen bonds requires the presence of water and hydrogen ions. These structural features have been used as supporting evidence for the hypotheses that crystallization occurs in an aqueous medium.^{17, 25, 28} Thus, it is evident that hemozoin crystallization

in an organic medium (e.g., lipid sub-phase of the DV) is feasible only if water is available in that environment.

Recent analyses indicate that the lipid structures in the DV of *P. falciparum* consist of monopalmitic, monostearic, dipalmitic, dioleic, and dilinoleic glycerols at molar ratios 2:4:1:1:1.^{15, 32} Since the lipid structures are in contact with the aqueous environment of the DV, it is feasible that they are saturated with water. To test this hypothesis, we determined the water solubility in a mixture of lipids representative of the DV blend using thermal gravimetric analysis (TGA).¹⁰ The results in Fig. 1 show a mass loss in lipid samples that plateaus between 70 and 85°C. Since these temperatures are significantly lower than the boiling points of the lipids, we conclude that the evaporated solvent component is water. The three traces in Fig. 1 indicate that the average amount of dissolved water in the lipid mixture is $8.5 \pm 0.5\%$ weight, corresponding to $4.2 \pm 0.3 \text{ mol kg}^{-1}$. This amount significantly exceeds the one needed to construct the hydrogen bonds in the hematin crystal structure, suggesting that water-saturated lipids could be a suitable medium for hematin crystallization.

The above lipid mixture is solid at room temperature (it is liquid at 37°C); hence, n-octanol has been suggested as a convenient biomimetic model.^{6, 33} Normal octanol is an amphiphilic molecule with a hydrophobic aliphatic tail of medium length and a hydrophilic polar head (-OH), which is smaller than the glycerol ester functional groups of the mono- and diglyceride lipids. Accordingly, water solubility in n-octanol (2.70 mol kg^{-1})³⁴ is lower than what was measured for the lipid mixture, but it is still sufficient for hydrogen bonding in hematin crystals. Octanol is routinely used to mimic lipids during determinations of the lipophilicity of drugs. Other model organic solvents that have been suggested in the literature are n-pentanol and monomyristoylglycerol (MMG).^{6, 33} Normal pentanol is similar to n-octanol, but with a shorter aliphatic chain and correspondingly lower hydrophobicity. Tests in our laboratory revealed that hematin crystal grown from n-pentanol are dendritic, in sharp contrast to the habit of hemozoin. MMG is solid at

temperatures up to 68 – 70°C, which sets it apart from the physiological lipid mixture. Herein, we use n-octanol saturated with citric buffer at pH 4.8 (which is within the range of pH in the DV)^{18, 19} as a model for the lipid mixture in the DV of malaria parasites; we refer to this solvent as CBSO.

Hematin and antimalarial drug solubility in organic and aqueous media

To determine the solubility of hematin in CBSO, we added 2 – 5 mM hematin powder to 5 mL CBSO held in a sealed glass vial. The vials were stored at constant temperature. Aliquots were removed and the concentration of dissolved hematin was determined spectrophotometrically. This procedure was repeated until the concentrations in each vial reached a plateau, defined by three consecutive readings of similar value.^{10, 35} Microscopic observations revealed that the initial amorphous hematin powder appeared to fully dissolve and β -hematin crystals with typical needle-like habit¹⁶ had formed. The steady concentration of this solution signifies equilibrium between the hematin crystals (and not amorphous hematin) and the solution. This concentration was used as the solubility of hematin in CBSO. The solubility determined using this bulk technique was consistent with a determination based on monitoring the growth and dissolution of steps on hematin crystal surfaces as a function of hematin concentration using atomic force microscopy (AFM).¹⁰

In Fig. 2 we compare the solubility of hematin in CBSO at 25°C to that in aqueous citric buffer at the same temperature and pH 4.8.³⁵ The data in Fig. 2 reveal that the solubility in CBSO is ca. 10^5 higher than in aqueous solutions. This is not surprising since hematin is highly hydrophobic. Given that crystal growth rates roughly scale with the solubility,³⁶ this disparity in the magnitude of hematin solubility indicates that crystallization from an organic phase is a significantly faster method of heme detoxification than from an aqueous phase.

An argument in the literature in favor of aqueous crystallization of hematin is the low solubility of the quinoline-class antimalarials in organic liquids, which would seemingly reduce their efficacy as inhibitors of crystals growing in a lipid phase. To quantitatively address the issue of antimalarial drug solubility in organic solvent, we measured the solubility of three common antimalarial drugs (chloroquine, amodiaquine and quinine) and two antibiotics employed in combination antimalarial therapies (doxycycline and sulfadoxine) in CBSO and citric buffer at pH 4.8. The data in Fig. 3 reveal that the solubilities of chloroquine and amodiaquine in CBSO are lower than that in aqueous solvent; however, they are significantly higher than the solubility of hematin in CBSO, ca. 0.2 mM. The solubilities of quinine, doxycycline, and sulfadoxine in CBSO are higher than their respective solubilities in the aqueous solvent and higher than the solubility of hematin in CBSO. The comparison between drug and hematin solubilities suggests that the five tested drugs can dissolve in CBSO with quantities that are sufficient for the inhibition of hematin crystallization. While we did not systematically determine the solubilities of additional antimalarials, such as pyronaridine, mefloquine, quinoline, and artemisinin, we performed preliminary bulk crystallization experiments using these compounds and observed that they also dissolve in organic solvents at concentrations sufficient for inhibition of hematin crystallization.

The growth of large hematin crystals from CBSO

The dimensions of hematin crystals *in vivo* are constrained by the size of the DV and the availability of hematin produced during digestion of hemoglobin. Hence, the largest hemozoin crystals extracted from the *P. falciparum* are less than 1 μm in their longest dimension.¹⁵ *In vitro*, both constraints are relaxed and one would expect significantly larger crystals to grow. As a test for the suitability of different environments for hematin crystallization, we attempted to grow hematin crystals larger than the physiological limit in purely aqueous, purely organic (anhydrous n-octanol), and CBSO solvents.

In aqueous solutions, we produced hematin crystals with longest dimension $\leq 3 \mu\text{m}$, achieving a marginal increase in crystal size, but only through the use of non-physiological conditions (i.e., ionic strength 0.5 – 5 M).³⁵ Our attempts to grow hematin crystals in aqueous solution using citric and acetate buffers (both at pH 4.8) as a surrogate for the DV produced crystals with a morphology distinctly different from that of hemozoin.³⁵ Representative AFM images of crystals grown in acetate buffer are presented in Fig. 4. The crystals exhibit block structure, illustrated in Fig. 4A. The entire surface area of the two twinned crystals in Fig. 4A, C, and D is rough. Sharp crystal edges, which are a signature of the crystallinity, are missing from all observed crystals. The crystals were often lamellar, as the one shown in Fig. 4C. The surface height profile in Fig. 4G along the dashed line in Fig. 4E demonstrates that the layer thickness varies from 12 to 63 nm. All layer heights are significantly greater than the thickness of a single crystal layer in the $(\bar{1}00)$ plane, which is 1.22 nm.³⁷ This inequality indicates that the layers observed in Fig. 4E are not growth steps, but rather elements of a mesoscopic lamellar structure. Such layered structures are an indication of growth under high elastic stress.³⁸ Another consequence of the elastic stress is severe twinning, which is known to impose unexpected crystal shapes³⁶ and is a potential mechanism for the unusual triangular crystals in Fig. 4C.

In summary, hematin crystals grown from aqueous solutions at pH 4.8 have unusual macroscopic and mesoscopic morphological features, which are incompatible with the shapes and surface features of biological hemozoin. This discrepancy cannot be attributed to impurity effects since impurities are abundant *in vivo*. Hence, one would expect rougher crystal shapes of biological hemozoin, which is in stark contrast to the actual observation. These considerations suggest that biological hemozoin crystals may not grow within a purely aqueous environment.

We then performed bulk crystallization studies using CBSO as a surrogate for the lipid sub-phase in the DV, as illustrated in Fig. 5A – C.³⁹ We placed ca. 2 mM hematin powder in direct contact with 5 mL freshly prepared CBSO. After three days, crystals of size 10 – 50 μm were observed at the

bottom of the container, Fig. 5D. The crystals were well faceted and had smooth faces with no visible gaps. To identify the primary faces, we used the published values of the dihedral angles.¹⁶ The crystal habit consists of {100}, {010}, (001) and $(0\bar{1}\bar{1})$ faces with ratios between their respective areas that are comparable to the hemozoin crystals found in *P. falciparum*, Fig. 5E.¹⁶ The powder X-ray diffraction (XRD) pattern of the grown crystal, Fig. 5F, is similar to those of hemozoin crystals extracted from the DV of *P. falciparum* and synthetic hematin crystals.¹⁶

To understand the sequence of processes leading to the growth of large hematin crystals, we analyzed the temporal evolution of the growth solution. Dynamic light scattering characterization of the CBSO solvent, top curve in Fig. 5G, revealed that it is not homogenous, but contains a relatively monodisperse population of scatters of size 120 nm (for details of this method, see Ketchum et al.,³⁵). When we diluted CBSO with anhydrous n-octanol, these scatterers disappeared, indicating that they are aqueous buffer droplets. We found that crystals do not nucleate in mixtures of citric buffer and n-octanol that are supersaturated with hematin unless water droplets are present. This observation suggests that the water – octanol interface promotes crystal nucleation. The higher solubility of hematin in octanol (Fig. 2) suggests that crystals most probably form in the octanol phase and not in the water droplets. It is reasonable to suggest that n-octanol molecules in contact with the water droplets orient with their -OH head groups toward the water and hematin crystals nucleate on the ordered layer of aliphatic tails. This scenario is similar to the hypothesis of hematin crystal nucleation on the aqueous side of a water – glyceride interface, assisted by a layer of ordered -OH groups^{16, 27, 40}, but differs in that we propose crystal nucleation occurs in the organic phase.

At later stages of crystal growth, when the hematin concentration increases due to further dissolution of amorphous hematin powder, the water droplets dissolve, as observed by DLS (Fig. 5G, lower curve). Our results reveal that both the organic and aqueous components are critical for crystal growth. For instance, hematin crystals failed to grow in anhydrous n-octanol, which agrees

with the hypothesis that H⁺ ions are a necessary component of the growth medium, presumably to facilitate the formation of hydrogen bonds in the crystal structure.^{15, 23, 37}

Growth of crystals in aqueous and organic biomimetic solvents

We employed *in situ* AFM to monitor the evolution of unfinished layers on large hematin crystals (prepared in CBSO) in the presence of multiple solvents. To mimic the aqueous environment in the DV of *P. falciparum*, we prepared solutions at low ionic strength. To simulate conditions used in previous studies of hematin crystallization,⁵ we also probed high ionic strengths. In addition, we tested several pH values in which growth solutions were prepared by adding hematin to the crystallization solution using two methods: dissolving in a 0.1 M NaOH and titrating to the desired pH, or placing solid hematin in the solvent, analogous to the CBSO solution preparation. We tested aqueous hematin solutions saturated with n-octanol to bring them closer to the composition in the parasite DV. In addition, we examined both filtered and unfiltered solutions to observe whether large aggregates forming in the solution might act as non-classical growth units and/or sites for heterogeneous nucleation.

For each growth solution composition, *in situ* AFM images revealed the dynamics of hematin crystal surfaces for over 48 hours. No surface processes leading to crystal growth were observed for any of the aforementioned solutions. In acidic solutions, immobile single steps were initially observed on the basal face, but they became obscured with increased time of exposure to the solution due to the deposition of an apparent coating (Fig. 6 A – C). In aqueous solutions, hematin is known to form several dimers and higher oligomers: the $\pi - \pi$ dimer (Fig. 6D) in which the Fe atoms in two parallel hematin monomers face outwards and are linked by overlapping π electron density; and the μ -oxo dimer (Fig. 6E) in which two hematin monomers are in parallel positions and their facing Fe atoms are bound by a O atom. As illustrated in Fig. 6E, larger oligomers can form when two or more μ -oxo dimers catenate by $\pi - \pi$ linkages.⁴¹ The structures of the soluble dimers

and oligomers are distinct from that of the head-to tail dimer (Fig. 6F), which exists in hematin crystals. It is feasible that any of the former three dimers and oligomers may be the species coating the surface in AFM images (Fig. 6C).

In basic solutions (i.e., high solubility of hematin)³⁵, the steps retreated, thereby indicating dissolution of the crystals. We did not detect any dynamic events that could allude to non-classical mechanisms (e.g., the deposition of precursors or aggregates followed by their restructuring to become part of the underlying crystal) in any of the tested aqueous solvents. A summary of all tested growth solution compositions and the observed surface behaviors in AFM studies is provided in Table 1.

In situ AFM observations revealed that in anhydrous n-octanol, in which the solubility of hematin is even greater than its value measured in CBSO,³⁵ steps retracted at hematin concentrations lower than the solubility, which is consistent with crystal dissolution. At concentrations higher than the solubility, continuous AFM scanning for 48 hours revealed no step growth or retreat, as shown in Fig. 7. Moreover, we did not observe the formation of an overlayer on the crystal surface, as was observed in acidic aqueous solutions (Fig. 6C).

In contrast, *in situ* AFM observations of hematin crystallization in CBSO reveal growth following a classical layer-by-layer mechanism wherein new crystal layers nucleate and grow by the attachment of solute molecules to advancing steps. The $(\bar{1}00)$ faces present unfinished layers of height $h = 1.17 \pm 0.07$ nm, close to the unit cell dimension in the $[100]$ direction $a = 1.22$ nm, Fig. 8.⁴ These layers nucleate, as illustrated in Fig. 8A and B, and their nucleation quantitatively complies with *a priori* predictions of classical nucleation theory.¹⁰ The layers spread by association of molecules to the steps, and this process follows first order kinetics with a step kinetic coefficient $\beta = 4.3 \mu\text{m s}^{-1}$ in the dominant growth direction and corresponding rate constant $k \cong 10^4 \text{ s}^{-1}$. Concentrations lower than the solubility result in step retreat, indicating dissolution of the hematin crystal.¹⁰

The rates of nucleation and growth of new crystal layers provide insight into hemozoin crystallization *in vivo*. Electron micrographs of hemozoin crystals in the parasite DV reveal that the crystals can reach thicknesses in the [100] direction of approximately 100 nm within 20 hours, corresponding to an average growth rate of about 10^{-3} nm s⁻¹. The combination of step velocity and step density can be used to approximate the hemozoin concentration required to achieve this growth rate, which we estimate to be close to 0.22 mM. This value is only slightly higher than the solubility of 0.16 mM, implying that hemozoin is sequestered into crystals soon after its release during hemoglobin digestion. Thus, even a moderate delay in crystallization may induce a significant accumulation of toxic hemozoin, leading to parasite eradication from its human host.

Nucleation and growth of hemozoin crystals *in vivo*

Here, we summarize the evidence that an organic phase is a preferred environment for the growth of hemozoin crystals. Hemozoin solubility is five orders of magnitude higher in organic solvent than in aqueous solutions that mimic the aqueous environment in the parasite DV. Since crystal growth rate roughly scales with solubility, crystallization from organic solvents is seemingly a more efficient means of heme detoxification. Many of the current antimalarial drugs are sufficiently soluble in the biomimetic CBSO solvent to ensure significant slowdown or complete cessation of hemozoin crystallization. The crystals grown in aqueous buffers are constrained to sizes ≤ 3 μm and are morphologically and structurally different from physiological hemozoin, whereas crystals as large as 50 μm possessing a morphology and powder XRD pattern similar to those of physiological hemozoin grown from the biomimetic CBSO solution. The unfinished layers on the surface of pre-grown hemozoin crystals do not appear to grow in aqueous solutions supersaturated with hemozoin; however, *in situ* AFM measurements in biomimetic CBSO supersaturated with hemozoin reveal the generation and growth of two-dimensional layers with growth rates that are generally consistent with our estimate of hemozoin growth rate *in vivo*.

This conclusion must be reconciled with the data on hemoglobin transport to the digestive vacuole, the digestion of hemoglobin and lipid, and heme release and detoxification *in vivo*^{17, 20-23, 25, 28} that demonstrate the following key points: (i) Hematin and neutral lipids are released in the aqueous sub-phase of the DV since the proteases and lipases that digest hemoglobin and the inner membranes of the hemoglobin transport vesicles are water-soluble; (ii) The synthesis of neutral lipids that are crucial for hematin crystal nucleation and growth is concomitant with the release of heme during hemoglobin digestion; (iii) The total volume of produced neutral lipids is about 1 fL; (iv) The released lipid droplets likely deposit on the DV membrane.

A mechanism of hematin crystallization in the parasite DV that reconciles the laboratory findings and the data on parasite physiology is suggested by the classical vapor-liquid-solid (VLS) crystallization mechanism,³⁶ illustrated in Fig. 9A. The VLS mechanism applies to crystals growing from their vapor. Since the molecular concentration in the vapor is low, the rate of growth directly from the vapor is slow. To accelerate crystallization, a drop of neutral liquid is deposited on a face of interest. The liquid is chosen such that the crystallizing compound is highly soluble in it. This leads to accumulation of molecules in the liquid drop and to correspondingly faster growth. Since the liquid is not incorporated in the crystal, the liquid drop is lifted with the growing interface, ensuring continuous crystallization.

We propose a mechanism of hematin crystallization analogous to the VLS growth mode wherein the role of vapor is taken by the aqueous medium, in which hematin is released. The liquid droplet in the VLS growth mode is then represented by lipids accumulated at the open crystal surfaces or at the interstice between the crystal and the underlying DV membrane. The proposed mechanism is illustrated in Fig. 9B. Crystals nucleate either on the phospholipid membrane of the DV^{17, 25, 28} or at the interface of neutral lipids, which may coat the DV membrane or embed in its phospholipid bilayer.^{16, 40, 42, 43} Hematin plates as large as $10 \times 10 \mu\text{m}^2$ embedded in biomimetic phospholipid bilayers have been observed.⁴⁴ Given that the solubility of hematin in the aqueous

solution is exceedingly low, hemozoin may be supplied to the nucleation site via two pathways: through a layer of neutral lipids that coat the membrane,²⁸ or through the DV membrane itself as hemozoin is significantly soluble in the two-dimensional environment of a phospholipid bilayer.⁴⁴

It is likely that the nucleated hemozoin crystals are coated by newly synthesized neutral lipids within the parasite DV. The surface of the hemozoin crystals is highly hydrophobic and can serve as a natural assembly site for the lipids. Their transport from the location of phospholipid hydrolysis may be enabled by their low, albeit finite, solubility in aqueous solutions. The thickness of the neutral lipid layer may be less than the detectable limit of analytical instruments (e.g., 25 nm), in particular around large crystals that are similar to those observed in mature trophozoites by Kapishnikov *et al.*^{17, 25, 28} The nucleated crystals grow from continuously released hemozoin, which diffuses through the aqueous solution, dissolves in the lipid, and associates to the crystals at the respective growth sites.¹⁰ Crystal growth is coordinated with the layer expansion by the concomitant generation of hemozoin and neutral lipids. An alternative pathway of hemozoin from the DV bulk to the crystal is via the DV membrane; this pathway is compatible with hemozoin crystallization exclusively through a lipid phase. The hemozoin crystal would mostly grow by molecular attachment to the basal ($\bar{1}00$) face that lifts the crystal into the DV.

The pharmacological consequences of this crystallization mechanism are significant. The primary implication is that potential antimalarial drugs that work by blocking hemozoin crystallization should be tested in water-saturated organic environments and not in purely aqueous solvents. Exploring the details of the transport of hemozoin from its synthesis in the aqueous sub-phase in the DV, through the lipid structures that underlie or shroud the hemozoin crystals, may offer valuable new targets for blocking crystallization and suppressing the parasite.

Several aspects of the proposed mechanism can be tested by high resolution electron microscopy and X-ray imaging of *P. falciparum* parasites. A direct confirmation would be to measure low hemozoin (free from hemoglobin) concentrations in the DV bulk and significantly

higher levels around growing crystals. This non-uniform distribution of hematin would suggest phase heterogeneity of the DV, compatible with a lipid layer coating the crystals. Determining the hematin concentrations embedded in the DV membrane could test the alternative crystallization pathway, discussed above.

Acknowledgements

We are deeply indebted to Sergey Kapishnikov, Leslie Leiserowitz, and David Sullivan for extensive discussions of hematin crystallization *in vivo* and in model solutions. This work was supported by NASA (NNX14AD68G and NNX14AE79G), NSF (Grant MCB-1244568), and The Welch Foundation (Grant E-1794).

References

1. D. E. Goldberg, A. F. Slater, A. Cerami and G. B. Henderson, *Proceedings of the National Academy of Sciences*, 1990, **87**, 2931-2935.
2. C. Fitch, R. Chevli, P. Kanjanangkulpan, P. Dutta, K. Chevli and A. Chou, *Blood*, 1983, **62**, 1165-1168.
3. R. G. Ridley, *Nature*, 2002, **415**, 686-693.
4. S. Pagola, P. W. Stephens, D. S. Bohle, A. D. Kosar and S. K. Madsen, *Nature* 2000, **404** 307-310.
5. T. J. Egan, D. C. Ross and P. A. Adams, *FEBS Lett.*, 1994, **352**, 54-57.
6. T. J. Egan, *Molecular and Biochemical Parasitology*, 2008, **157**, 127-136.
7. K. A. de Villiers and T. J. Egan, *Molecules*, 2009, **14**, 2868-2887.
8. J. Soares, D. Menezes, M. A. Vannier-Santos, A. Ferreira-Pereira, G. T. Almeida, T. M. Venancio, S. Verjovski-Almeida, V. K. Zishiri, D. Kuter, R. Hunter, T. J. Egan and M. F. Oliveira, *Plos Neglect. Trop. Dis.*, 2009, **3**.
9. D. J. Sullivan, *Int J Parasitol*, 2002, **32**, 1645-1653.
10. F. C. Meldrum and H. Cölfen, *Chemical Reviews*, 2008, **108**, 4332-4432.
11. R. T. Eastman and D. A. Fidock, *Nat Rev Microbiol*, 2009, **7**, 864-874.
12. WHO, *Malaria Fact Sheet No 94*, World Health Organization, 2015.
13. C. P. Sanchez, A. Dave, W. D. Stein and M. Lanzer, *Int J Parasitol*, 2010, **40**, 1109-1118.
14. D. S. Bohle, R. E. Dinnebier, S. K. Madsen and P. W. Stephens, *J. Biol. Chem.*, 1997, **272**, 713-716.
15. J. M. Pisciotta, I. Coppens, A. K. Tripathi, P. F. Scholl, J. Shuman, S. Bajad, V. Shulaev and D. J. Sullivan, *Biochem. J.*, 2007, **402**, 197-204.
16. I. Weissbuch and L. Leiserowitz, *Chemical Reviews*, 2008, **108**, 4899-4914.
17. S. Kapishnikov, A. Weiner, E. Shimoni, P. Guttmann, G. Schneider, N. Dahan-Pasternak, R. Dzikowski, L. Leiserowitz and M. Elbaum, *Proceedings of the National Academy of Sciences of the United States of America*, 2012, **109**, 11188-11193.
18. B. Gligorijevic, T. Bennett, R. McAllister, J. S. Urbach and P. D. Roepe, *Biochemistry*, 2006, **45**, 12411-12423.
19. R. Hayward, K. J. Saliba and K. Kirk, *Journal of Cell Science*, 2006, **119**, 1016-1025.

20. I. Stranski and D. Totomanov., *Z. phys. Chem.*, 1933, **A163** 399-408.
21. Y. N. Palyanov, A. F. Khokhryakov, Y. M. Borzdov and I. N. Kupriyanov, *Crystal Growth & Design*, 2013, **13**, 5411-5419.
22. W. Ostwald, *Z. phys. Chem.*, 1897, **22**, 289-330.
23. M. A. Vorontsova, D. Maes and P. G. Vekilov, *Faraday Discussions*, 2015, **179**, 27-40.
24. M. Krugliak, J. Zhang and H. Ginsburg, *Molecular and Biochemical Parasitology*, 2002, **119**, 249-256.
25. S. Kapishnikov, A. Weiner, E. Shimoni, G. Schneider, M. Elbaum and L. Leiserowitz, *Langmuir*, 2013, **29**, 14595-14602.
26. S. Price, S. Veessler, H. Pan, K. Lewtas, M. Smets, B. Rimez, A. Myerson, C. Hughes, A. Hare, F. Zhang, H. Meekes, M. Mazzotti, I. Rosbottom, D. Khamar, J. van den Ende, L. Fabian, S. Black, F. Taulelle, M. Gich, P. Vekilov, D. Toroz, C. A. Bertran, J. Sefcik, S. Schroeder, S. Booth, A. Rasmuson, E. Breynaert, E. Simone, R. Hammond, R. Sear, J. de Yoreo, R. Davey, J. Anwar, R. Ristic, D. M. Camacho Corzo, K. Roberts, K. Harris, H. Colfen and T. Turner, *Faraday Discussions*, 2015, **179**, 155-197.
27. A. Sauter, F. Roosen-Runge, F. Zhang, G. Lotze, A. Feoktystov, R. M. J. Jacobs and F. Schreiber, *Faraday Discussions*, 2015, **179**, 41-58.
28. S. Kapishnikov, T. Berthing, L. Hviid, M. Dierolf, A. Menzel, F. Pfeiffer, J. Als-Nielsen and L. Leiserowitz, *Proceedings of the National Academy of Sciences of the United States of America*, 2012, **109**, 11184-11187.
29. A. N. Hoang, K. K. Ncokazi, K. A. de Villiers, D. W. Wright and T. J. Egan, *Dalton Trans*, 2010, **39**, 1235-1244.
30. A. N. Hoang, R. D. Sandlin, A. Omar, T. J. Egan and D. W. Wright, *Biochemistry*, 2010, **49**, 10107-10116.
31. M. A. Ambele and T. J. Egan, *Malar J*, 2012, **11**, 337.
32. N. T. Huy, A. Maeda, D. T. Uyen, D. T. X. Trang, M. Sasai, T. Shiono, T. Oida, S. Harada and K. Kamei, *Acta Tropica*, 2007, **101**, 130-138.
33. T. J. Egan, *J. Inorg. Biochem.*, 2008, **102**, 1288-1299.
34. N. Šegatin and C. Klofutar, *Monatshefte für Chemie / Chemical Monthly*, 2004, **135**, 241-248.
35. M. A. Ketchum, K. N. Olafson, E. V. Petrova, J. D. Rimer and P. G. Vekilov, *The Journal of Chemical Physics*, 2013, **139**, 121911.
36. A. A. Chernov, *Modern Crystallography III, Crystal Growth*, Springer, Berlin, 1984.
37. R. Buller, M. L. Peterson, O. Almarsson and L. Leiserowitz, *Crystal Growth & Design*, 2002, **2**, 553-562.
38. A. A. Chernov, *J. Crystal Growth*, 1999, **196**, 524-534.
39. K. N. Olafson, J. D. Rimer and P. G. Vekilov, *Crystal Growth & Design*, 2014, **14**, 2123-2127.
40. K. A. de Villiers, M. Osipova, T. E. Mabothe, I. Solomonov, Y. Feldman, K. Kjaer, I. Weissbuch, T. J. Egan and L. Leiserowitz, *Crystal Growth & Design*, 2008, **9**, 626-632.
41. C. Asher, K. A. de Villiers and T. J. Egan, *Inorg Chem*, 2009, **48**, 7994-8003.
42. K. A. de Villiers, M. Osipova, T. E. Mabothe, I. Solomonov, Y. Feldman, K. Kjaer, I. Weissbuch, T. J. Egan and L. Leiserowitz, *Crystal Growth & Design*, 2009, **9**, 626-632.
43. I. Solomonov, M. Osipova, Y. Feldman, C. Baetz, K. Kjaer, I. K. Robinson, G. T. Webster, D. McNaughton, B. R. Wood, I. Weissbuch and L. Leiserowitz, *Journal of the American Chemical Society*, 2007, **129**, 2615-2627.
44. Y. Qutub, V. Uzunova, O. Galkin and P. G. Vekilov, *J. Phys. Chem. B*, , 2010, **114**, 4529-4535.
45. G. S. Noland, N. Briones and D. J. Sullivan Jr, *Molecular and Biochemical Parasitology*, 2003, **130**, 91-99.

Table 1.Aqueous solutions examined as putative growth media for β -hematin crystallization

Growth Medium	Solution Parameters	Hematin Source	Hematin Concentration	<i>In situ</i> AFM Observations
Acidic, low ionic strength	25 mM citric buffer, pH 4.80	hematin dissolved in 0.1 M NaOH, pH 13	< 2 nM	no step growth or dissolution
	25 mM citric buffer, pH 3.5	solid hematin, 2 mM	< 2 nM	no step growth or dissolution
Acidic, high ionic strength	4.5 M ammonium acetate, pH 4.80	hematin dissolved in 0.1 M NaOH, pH 13	< 0.1 mM	no step growth or dissolution
Basic	0.1 M NaOH, pH 13	none	0 mM	step dissolution
	0.1 M NaOH, pH 13	hematin dissolved in 0.1 M NaOH, pH 13	0 mM	step dissolution
	0.1 M NaOH, pH 10	none	0 mM	step dissolution
Acidic solution saturated with organic solution	25 mM citric buffer, pH 4.80; saturated with n-octanol	none	0 mM	step dissolution
		solid hematin	< 0.1 mM	no step growth or dissolution
		hematin dissolved in 0.1 M NaOH, pH 13	< 0.1 mM	no step growth or dissolution

Figure Captions

Figure 1. Solubility of water in a lipid mixture representative of the composition of the neutral lipids in the parasite DV: monopalmitic, monostearic, dipalmitic, dioleic, and dilinoleic glycerols at molar ratios 2:4:1:1:1. The mass fraction of evaporated solvent, determined by thermogravimetric analysis (TGA) is plotted as a function of temperature at three temperature ramp rates, labeled i to iii.

Figure 2. Comparison of the solubility at 25°C of hematin in citric buffer saturated n-octanol (CBSO) and aqueous citric buffer at pH = 4.8.

Figure 3. The solubility at 25°C of three antimalarial drugs, amodiaquine (AQ), quinine (QN), and chloroquine (CQ), and two commonly used antibiotics, sulfadoxine (SD) and doxycycline (DC), in citric buffer saturated n-octanol (CBSO), top, and aqueous citric buffer at pH = 4.8, bottom.

Figure 4. AFM analysis of the surface structure of hematin crystals grown in aqueous solutions at pH = 4.8. **A.** Low magnification view of two crystals consisting of individual blocks; dashed lines highlight block boundary. **B.** High magnification view of the surface of a crystal showing rounded formations. **C.** A crystal with apparent lamellar structure, indicated by arrows. **D.** High resolution image of the area highlighted by a white square in C shows rounded formations similar to those in B. **E.** A crystal with a relatively smooth surface around the white square and a rough area covering more than 80 % of the top face. **F.** A high resolution image of area highlighted by a square in E showing that the apparently smooth area consists of lamellar layers. **G.** Surface profile along dashed line in E. The thicknesses of the layers are shown in nanometers. Reprinted from Ketchum et al.³⁵ with permission from AIP.

Figure 5. The growth of large hematin crystals from citric buffer saturated octanol (CBSO). **A.** A CBSO sample is placed in contact with amorphous hematin. **B.** Amorphous hematin dissolves and hematin crystals nucleate at the interfaces of citric buffer droplets. **C.** As the concentration of soluble hematin increases, the water solubility in n-octanol increases and the aqueous droplets suspended in CBSO dissolve. During this time, hematin crystals continue to grow and gradually sediment. **D.** An AFM image of a crystal that was prepared using the procedure illustrated in A – C. **E.** Transmission electron microscopy images of crystals extracted from *P. falciparum*, reprinted from Noland et al. ⁴⁵ with permission from Elsevier. **F.** Powder X-ray diffraction (XRD) patterns of hematin: top, a model pattern computed using the software package Diamond and hematin structure coordinates from the Cambridge Structural Database; middle, crystals grown in the laboratory following the procedure illustrated in A – C; and bottom, hematin reagent from Sigma Aldrich (as received), indicating that the commercial material is predominately amorphous. **G.** Correlation functions from CBSO samples analyzed by dynamic light scattering (DLS). Upper curve: from CBSO prior to introduction of hematin reveals the presence of droplets of aqueous citric buffer of radius $R \cong 120$ nm, as schematically depicted in A. The lower curve provides evidence of droplet dissolution after one day of crystal growth.

Figure 6. The crystal surface in biomimetic aqueous solvents. **A – C.** Time-resolved AFM images reveal the evolution of the surface of a crystal grown in CBSO after insertion in aqueous citrate buffer at pH 4.8. The steps on the surface do not move indicating that molecules do not incorporate into them at a significant rate. After 9.5 hr, the surface is coated with a residue that may consist of hematin dimers and higher order oligomers. **C.** The residue persists after an additional 13.5 hr of imaging. **D and E.** The structures of a π - π dimer and of stacked μ -oxo dimers, respectively. **F.** The structure of the head-to-tail dimer existing in physiological and synthetic hematin crystals.

Figure 7. AFM images of a (100) hematin surface in an anhydrous n-octanol solution containing 0.55 mM hematin. Continuous imaging for approximately 40 min reveals that the steps neither propagate nor dissolve.

Figure 8. The evolution of the surface features on a (100) hematin surface in CBSO with hematin concentration 0.21 mM. The step indicated with the arrow in A (labelled *i*) grows upward. An example of new islands that nucleate and grow is indicated with the arrow in B (labelled *ii*).

Figure 9. A. The vapor-liquid-solid (VLS) mechanism of crystal growth. **B.** Schematic illustration of the proposed aqueous – lipid – solid (ALS) mechanism of hematin crystallization in the parasite DV. The parasite, enveloped in a double membrane, resides in a red blood cell. Hematin and neutral lipids (dioleic glycerol is shown) are synthesized in the aqueous sub-phase during the digestion of, respectively, hemoglobin and hemoglobin transport vesicle membranes. Hematin crystals nucleate on the DV membrane and remain attached to the membrane bilayer during growth. Hematin likely reaches the crystal by one of two pathways: dissolving into a shroud of neutral lipids that coats the crystals, or penetrating the phospholipid bilayer of the DV membrane.

TOC Text

Hematin crystallization, the primary heme detoxification mechanism of malaria parasites infecting human erythrocytes, most likely requires the participation of lipid structures.

Biographical Sketches

Peter Vekilov received his PhD in 1991 from the Russian Academy of Sciences. He is now John and Rebecca Moores Professor of Chemical and Biomolecular Engineering and of Chemistry at the University of Houston. His main research interests are in the area of phase transitions in solutions and aggregation of biological molecules. Peter is a 2014 – 2016 Francqui International Professor, a Fellow of the American Physical Society, and a recipient of several national and international prizes. He has served as President of the International Organization for Biological Crystallization and is a member of the Executive Committee of the American Crystal Growth Association.

Jeffrey Rimer is the Ernest J. and Barbara M. Henley Assistant Professor of Chemical Engineering at the University of Houston. Rimer received his Ph.D. in Chemical Engineering from the University of Delaware in 2006. Prior to joining the Department of Chemical and Biomolecular Engineering at Houston in 2009, he spent two years as a postdoctoral fellow at New York University's Molecular Design Institute within the Department of Chemistry. Rimer's research in crystal engineering focuses on the design of materials with specific applications in the synthesis of microporous catalysts and adsorbents, and the development of therapeutics to inhibit crystal formation in pathological and infectious diseases.

Katy N. Olafson was born in Kentucky where she received her Bachelor of Science in Chemical Engineering in 2012 from the University of Louisville J.B. Speed School of Engineering. She is currently a PhD candidate at the University of Houston where her research focuses on the

fundamental mechanisms of hemozoin crystallization that underlies malaria pathophysiology and the mode of inhibition by antimalarials.

Megan A. Ketchum earned her bachelor's degree from the Chemical & Petroleum Engineering Department at the University of Kansas in 2012. She is now a doctoral student at the University of Houston with an expected graduation date of early 2017. Megan studies the fundamental crystallization mechanisms of hemozoin and other biological molecules and aims to develop methods to evaluate the efficacy of drugs targeting malaria and similar pathologies.

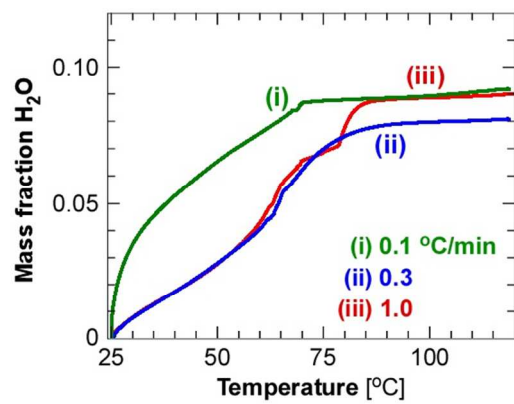


Figure 1.

190x254mm (300 x 300 DPI)

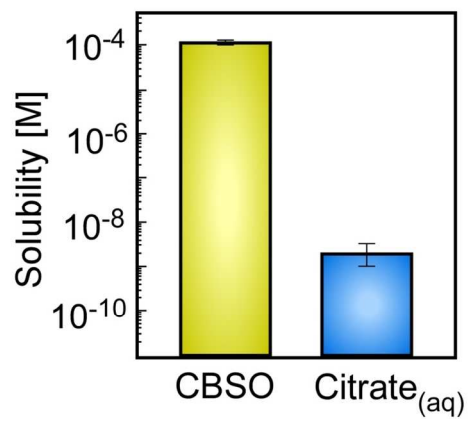


Figure 2.

190x254mm (300 x 300 DPI)

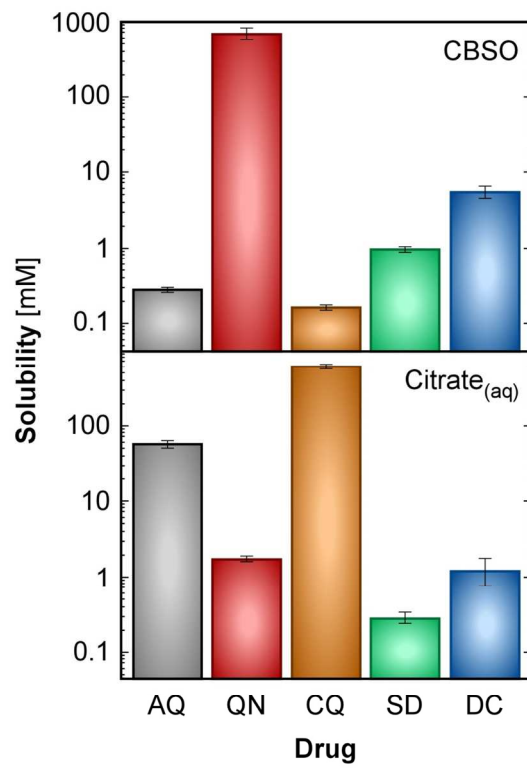


Figure 3.

190x254mm (300 x 300 DPI)

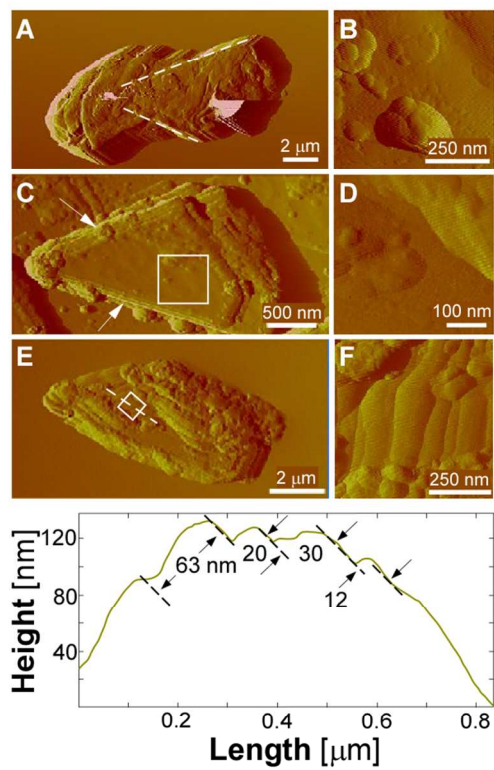


Figure 4.

190x254mm (300 x 300 DPI)

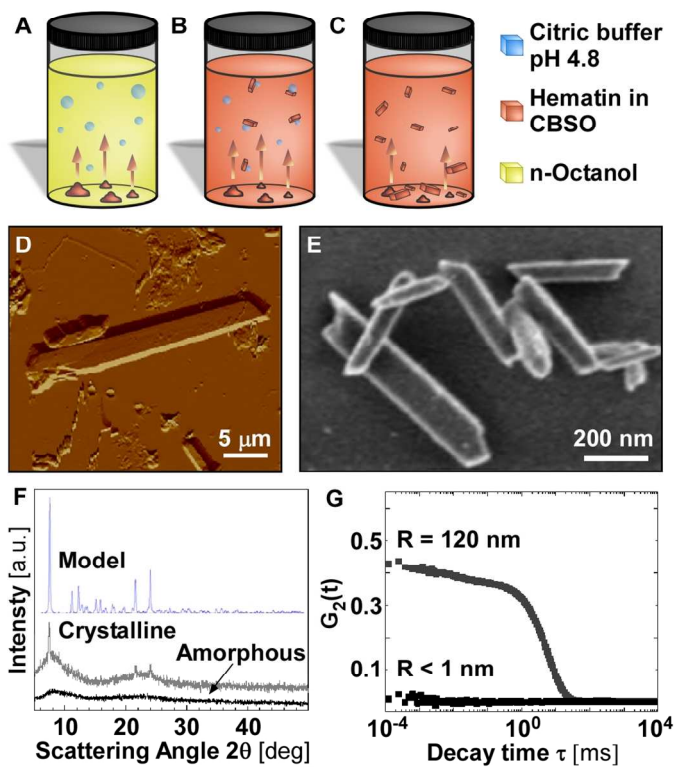


Figure 5.

190x254mm (300 x 300 DPI)

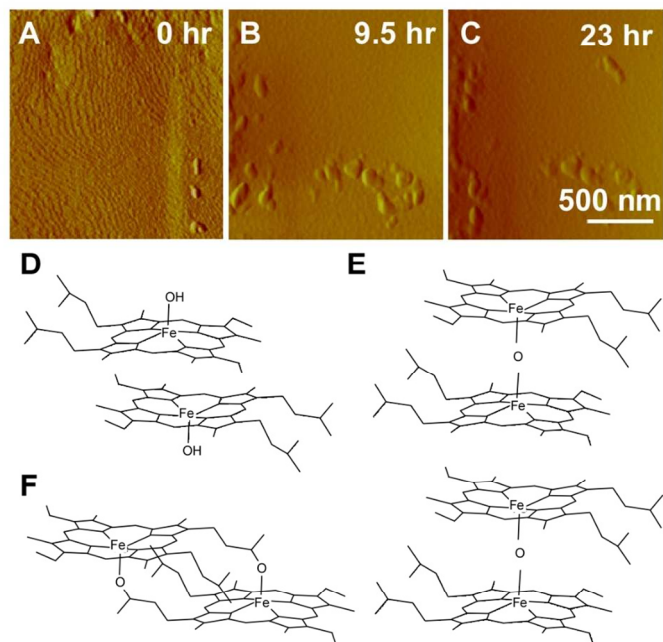


Figure 6.

190x254mm (300 x 300 DPI)

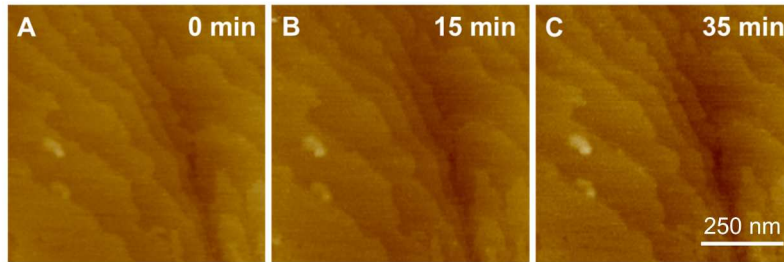


Figure 7.

190x254mm (300 x 300 DPI)

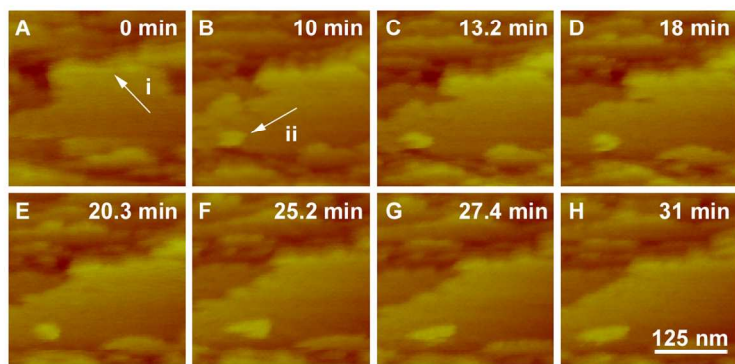
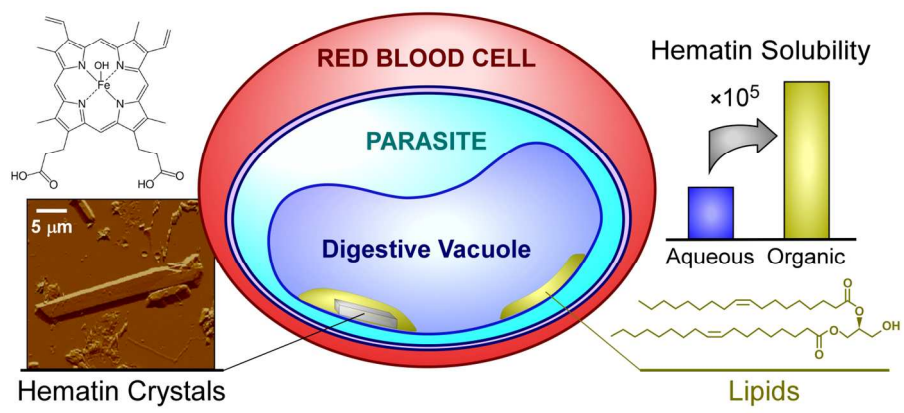


Figure 8.

190x254mm (300 x 300 DPI)



Hematin Crystals

TOC

190x254mm (300 x 300 DPI)